Chapter 1

Investigation into the Behavior of Metasurface by Modal Analysis

Mohsen Kalantari

Additional information is available at the end of the chapter

http://dx.doi.org/10.5772/intechopen.80584

Abstract

The existence of metasurface, in the way of propagating wave, affects the wave by blocking some of the incident power. In this chapter, modal analysis is used to analyze a metasurface structure, which is a two-dimensional periodic structure. First, the structure is modeled by an element inside the TEM waveguide. In the following, the reflected and transmitted waves are expanded by different modes, potentially propagated along the TEM waveguide. The key parameters in determining the behavior of structure are specified. The effect of each parameter in behavior of the structure is shown. This technique is used for different metasurfaces, and simulation results are presented in the chapter. This technique is extended to multilayer metamaterial structures.

Keywords: metamaterial layer, metasurface, periodic structure, modal analysis

1. Introduction

The appearance of metamaterial sun on the horizon of electromagnetic field results to/into absorbing most researchers to them (directing most researches into them). Although these structures were used a long time ago, it did not take a long time from when the metamaterial was introduced. Ref. [1] reviews a brief history about metamaterial structures over time. The importance of metamaterials is hidden behind (due to) their behaviors. The ability to control the refractive index, in other words constitutive parameters, of metamaterials leads into their interest behaviors [1, 2]. These structures help engineers to design new devices and improve the performance of available systems. Some of them are THz detectors, new substrate, modulator, THz switches, cloaking, bolometers, and angular-independent surfaces [2].

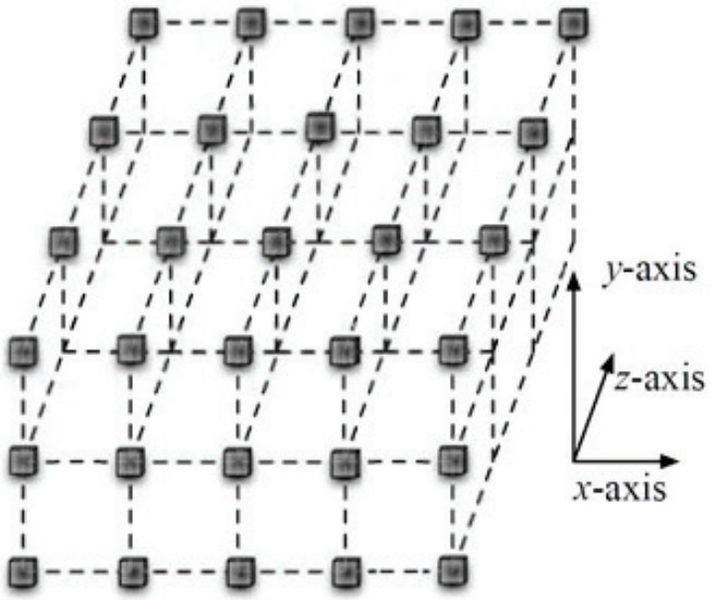

Figure 1. A metamaterial structure consisted of micro-scatterers in a regular array (reproduced from [1]).

Generally, a metamaterial is a periodic structure that is made from arranging a lot of the same micro-scatterers in a regular lattice/network (**Figure 1**) [1, 2]. A metamaterial layer is created when micro-scatterers are distributed in a plane. The difference between metamaterials and other periodic structures is mentioned in [2].

Impinging a wave into the metamaterial structure induces currents and charges on the metamaterial elements. In other words, the existence of metamaterial elements reinforces the structure in the (electric and magnetic) polarization. There are different methods developed to determine this polarization. In the following, we discuss about these methods. Then the structure is modeled and analyzed by modal analysis to calculate the S parameters of structure. These parameters show the general behavior of structure.

2. Modeling metamaterial structure

Some methods are developed to determine the effective parameters of these structures. The electromagnetic properties of an inhomogeneous composite can be determined exactly by solving Maxwell's equations, which relate the local electric and magnetic fields to the local charge and current densities. To solve this set of equations, a relationship must be assumed that relates the four macroscopic field vectors that arise from the averaging or homogenization procedure [3].

On the other hand, many researchers have in practice used an approach based upon the reflection and transmission coefficients of a metamaterial sample of some defined thickness [2]. The Nicolson-Ross-Weir (NRW) approach is then used to obtain the effective material properties of the bulk metamaterials. The solution of equation in this method is dependent on

square root function. Typically, the choice of the sign of a square root is made unambiguous by ensuring positive power flow in the direction of propagation [2]. In some situations, local effects near the boundaries of the sample must also be taken into account.

In contrast, there are some metasurface studies that have modeled the film as a single-layer metamaterial. In this way, a metasurface is replaced with a boundary plane with surface susceptibilities. It is called the Generalized Sheet Transition Condition (GSTC) [2, 4, 5].

3. Analysis of a periodic structure with modal analysis

As mentioned above, a metasurface is a periodic structure that is comprised from distributing a lot of micro-scatterers on a plane (**Figure 2a**). Therefore, for extracting the behavior of structure, it is sufficient to consider a period of structure with suitable boundary conditions [6]. **Figure 2b** shows these boundary conditions. These are two perfect electric conductors and two perfect magnetic conductors. On the other hand, these boundary conditions form/constitute a TEM waveguide, and the metasurface element in the middle is a transverse discontinuity in the waveguide. The element divides the inner medium of the waveguide into two media, medium I and medium II (**Figure 2c**).

Now, this model must be analyzed by a numerical technique such as mode matching, FDTD, or so on [7–12]. Generally, the element (partially) blocks the way of incident power ($P_{incident}$). It causes some of the incident power passes through discontinuity toward load ($P_{transmitted}$), and the remaining power reflects back to the source ($P_{reflected}$). In mathematical form (Eq. 1)

$$P_{incident} = P_{reflected} + P_{transmitted} \tag{1}$$

According to mode-matching method, the reflected and transmitted waves are expanded in terms of different modes supported by TEM waveguide (Eqs. 2–4) [7]. These modes are mentioned in Eqs. 2–5:

$$\vec{E}^i = \hat{a}_y A_{00}, \quad \vec{H}^i = -\hat{a}_x \frac{A_{00}}{\eta_0} \tag{2}$$

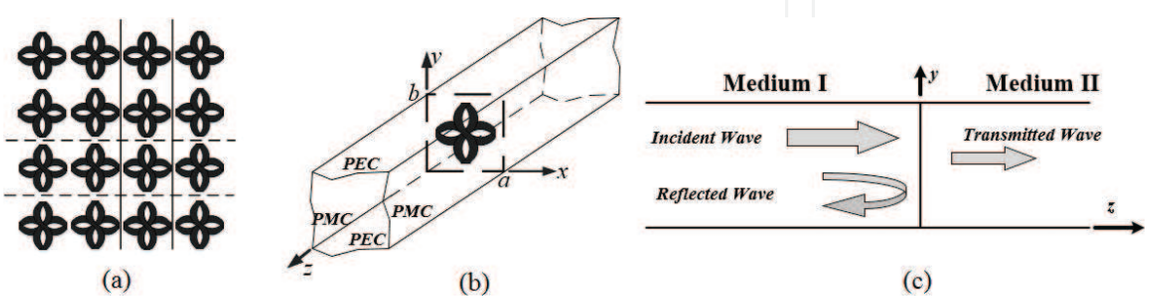

Figure 2. Front view of a metasurface structure (a) a TEM waveguide with a metasurface element in the middle (b) and incident, reflected, and transmitted waves in the TEM waveguide from side view (c) [7].

$$\vec{E}^r = \hat{a}_x \sum_{k=TE,TM} \sum_{m,n} \left(E_x^r\right)_{mn}^k e^{j\beta_{mn}z} + \hat{a}_y \left(a_{00} e^{j\beta_{00}z} + \sum_{k=TE,TM} \sum_{m,n} \left(E_y^r\right)_{mn}^k e^{j\beta_{mn}z} \right) + \hat{a}_z E_z^r$$

$$\vec{H}^r = \hat{a}_x \left(\frac{a_{00}}{\eta_0} e^{j\beta_{00}z} + \sum_{k=TE,TM} \sum_{m,n} \frac{\left(E_y^r\right)_{mn}^k}{Z_{mn}^k} e^{j\beta_{mn}z} \right) - \hat{a}_y \left(\sum_{k=TE,TM} \sum_{m,n} \frac{\left(E_x^r\right)_{mn}^k}{Z_{mn}^k} e^{j\beta_{mn}z} \right) + \hat{a}_z H_z^r \tag{3}$$

$$\vec{E}^t = \hat{a}_x \sum_{k=TE,TM} \sum_{m,n} \left(E_x^t\right)_{mn}^k e^{-j\beta_{mn}z} + \hat{a}_y \left(c_{00} e^{-j\beta_{00}z} + \sum_{k=TE,TM} \sum_{m,n} \left(E_y^t\right)_{mn}^k e^{-j\beta_{mn}z} \right) + \hat{a}_z E_z^t$$

$$\vec{H}^t = \hat{a}_x \left(-\frac{c_{00}}{\eta_0} e^{-j\beta_{00}z} - \sum_{k=TE,TM} \sum_{m,n} \frac{\left(E_y^t\right)_{mn}^k}{Z_{mn}^k} e^{-j\beta_{mn}z} \right) - \hat{a}_y \left(\sum_{k=TE,TM} \sum_{m,n} \frac{\left(E_x^t\right)_{mn}^k}{Z_{mn}^k} e^{-j\beta_{mn}z} \right) + \hat{a}_z H_z^t \tag{4}$$

where $\vec{E}^i$, $\vec{E}^r$, and $\vec{E}^t$ are incident, reflected, and transmitted electric fields, respectively. This is right about $\vec{H}^i$, $\vec{H}^r$, and $\vec{H}^t$, the incident, reflected, and transmitted magnetic fields, respectively.

$$\beta_{mn} = \sqrt{\omega^2 \mu_0 \varepsilon_0 \varepsilon_r - \left(\frac{m\pi}{a}\right)^2 - \left(\frac{n\pi}{b}\right)^2} \ , \quad Z_{mn}^{TE} = \frac{\omega\mu_0}{\beta_{mn}} \ , \quad Z_{mn}^{TM} = \frac{\beta_{mn}}{\omega\varepsilon_0\varepsilon_r} \tag{5}$$

$$TEM : \begin{cases} E_x^i = 0 \\ E_y^i = A_{00} \end{cases} , \quad \begin{cases} H_x^i = -\dfrac{A_{00}}{\eta_0} \\ H_y^i = 0 \end{cases} \tag{6}$$

$$TM : \begin{cases} (E_x)_{mn} = \dfrac{m\pi}{a} a_{mn} \varphi_{mn}(x,y) \ , \ (H_x)_{mn} = -\dfrac{(E_y)_{mn}}{Z_{mn}^{TM}} \\ (E_y)_{mn} = -\dfrac{n\pi}{b} a_{mn} \psi_{mn}(x,y), \ (H_y)_{mn} = \dfrac{(E_x)_{mn}}{Z_{mn}^{TM}} \end{cases} \tag{7}$$

$$TE : \begin{cases} (E_x)_{mn} = \dfrac{n\pi}{b} b_{mn} \varphi_{mn}(x,y) \ , \ (H_x)_{mn} = -\dfrac{(E_y)_{mn}}{Z_{mn}^{TE}} \\ (E_y)_{mn} = \dfrac{m\pi}{a} b_{mn} \psi_{mn}(x,y), \ (H_y)_{mn} = \dfrac{(E_x)_{mn}}{Z_{mn}^{TE}} \end{cases} \tag{8}$$

$$\varphi_{mn}(x,y) \triangleq \sin\left(\frac{m\pi}{a}x\right) \sin\left(\frac{n\pi}{b}y\right) \ , \quad \psi_{mn}(x,y) \triangleq cos\left(\frac{m\pi}{a}x\right) cos\left(\frac{n\pi}{b}y\right). \tag{9}$$

where β_{mn}, Z_{mn}^{TE}, and Z_{mn}^{TM} are propagation constant, characteristic impedance of TE mode, and characteristic impedance of TM mode, respectively. For determining the weights of each mode, the boundary conditions must be applied on the transverse plane (Eq. 5) [7, 13–20]. These boundary conditions include vanishing transverse electric field on the metal element (R_m) and

continuity of electric and magnetic fields in the aperture (R_m^c). R_m^c is all the remaining parts of a transverse plane except R_m:

$$\left(\vec{E}^i + \vec{E}^r\right)_t = \begin{cases} 0 & R_m \\ \left(\vec{E}^t\right)_t & R_m^c \end{cases}, \quad \left(\vec{H}^i + \vec{H}^r\right)_t = \begin{cases} 0 & R_m \\ \left(\vec{H}^t\right)_t & R_m^c \end{cases} \tag{10}$$

Note that the tangential components of an electric field are continuously passing through the metal transverse discontinuity [7, 13, 21]:

$$\left(\vec{E}^i + \vec{E}^r\right)_t = \left(\vec{E}^t\right)_t \quad \rightarrow \quad \begin{cases} c_{mn} = a_{mn} + A_{00}\delta_{m0}\delta_{n0} \\ d_{mn} = b_{mn} \end{cases} \quad m, n = 0, 1, 2, \ldots \tag{11}$$

4. The variation in S parameters for a metasurface

Considering Eq. 11 for TEM mode (m = n = 0)

$$c_{00} = a_{00} + A_{00} \quad \rightarrow \quad \frac{c_{00}\Big/\sqrt{(\eta_0)_{II}}}{A_{00}\Big/\sqrt{(\eta_0)_I}} = \frac{a_{00}\Big/\sqrt{(\eta_0)_I}}{A_{00}\Big/\sqrt{(\eta_0)_I}} + 1 \rightarrow s_{21} = \sqrt{\frac{(\eta_0)_{II}}{(\eta_0)_I}}(1 + s_{11}) = s_{12} \tag{12}$$

where equality between s_{21} and s_{12} are resulted from reciprocity. Rewriting Eq. 12 for exciting waveguide from transmitted media in **Figure 2c** [7],

$$s_{21} = s_{12} = \sqrt{\frac{(\eta_0)_I}{(\eta_0)_{II}}}(1 + s_{22}) \rightarrow s_{22} = \frac{(\eta_0)_I}{(\eta_0)_{II}}(1 + s_{11}) - 1 \tag{13}$$

Suppose that the metasurface element is lossless. Rewriting Eq. 1;

$$P_{incident} = P_{reflected} + P_{transmitted} \rightarrow 1 = |s_{11}|^2 + |s_{21}|^2 \tag{14}$$

Considering Eqs. 12–14 simultaneously result into [7],

$$\left\{\mathrm{Re}(s_{11}) + \frac{(\eta_{00})_I}{(\eta_{00})_I + (\eta_{00})_{II}}\right\}^2 + \{\mathrm{Im}(s_{11})\}^2 = \left\{\frac{(\eta_{00})_{II}}{(\eta_{00})_I + (\eta_{00})_{II}}\right\}^2 \tag{15}$$

Eq. 15 is a relation of a circle on the complex plane of reflection coefficient (Smith chart). The center and radius of this circle are $[-(\eta_{00})_I/((\eta_{00})_I + (\eta_{00})_{II}), 0]$ and $(\eta_{00})_{II}/((\eta_{00})_I + (\eta_{00})_{II})$, respectively. This circle crosses horizontal axis in two points: $[-1, 0]$ and $[((\eta_{00})_{II} - (\eta_{00})_I)/((\eta_{00})_{II} + (\eta_{00})_I), 0]$. The first point is corresponding to when a metal plate covers the boundary between two media. The second point happens when two media touch each other completely without any element on the boundary. In this case, the reflection coefficient is

$((\eta_{00})_{II} - (\eta_{00})_{I})/((\eta_{00})_{II} + (\eta_{00})_{I})$. It is important that the s_{11} is coincided on this circle (Eq. 15), regardless of the geometrical shape of the element. Rewriting Eq. 15 in terms of center and radius of circle,

$$S_{11} = a_1 + r_1 e^{j\theta} \quad , \quad a_1 = \frac{-(\eta_{00})_I}{(\eta_{00})_{II} + (\eta_{00})_I} \quad , \quad r_1 = \frac{(\eta_{00})_{II}}{(\eta_{00})_{II} + (\eta_{00})_I} \quad , \quad r_1 = 1 + a_1 \tag{16}$$

r_1 and a_1 are functions of constitutive parameters of two media that surround the metasurface. The geometrical properties of metasurface (size and shape) determine the parameter θ. The circles corresponding to s_{21} and s_{22} are

$$\left\{ \mathrm{Re}(s_{22}) + \frac{(\eta_{00})_{II}}{(\eta_{00})_I + (\eta_{00})_{II}} \right\}^2 + \{\mathrm{Im}(s_{22})\}^2 = \left\{ \frac{(\eta_{00})_I}{(\eta_{00})_I + (\eta_{00})_{II}} \right\}^2 \tag{17}$$

$$\left\{ \mathrm{Re}(s_{21}) - \frac{\sqrt{(\eta_{00})_I (\eta_{00})_{II}}}{(\eta_{00})_I + (\eta_{00})_{II}} \right\}^2 + \{\mathrm{Im}(s_{21})\}^2 = \left\{ \frac{(\eta_{00})_I (\eta_{00})_{II}}{\left((\eta_{00})_I + (\eta_{00})_{II}\right)^2} \right\} \tag{18}$$

The point [−1, 0] is a common point between s_{11} and s_{22} circles. The s_{21} circle is located on the right-hand side of the Smith chart.

5. Simulation results

In this section, simulation results of a few examples of metasurface are demonstrated. All examples are simulated by modal analysis (in MATLAB). Simulation results are repeated by finite element method (FEM) (in HFSS). In the following simulations, it is supposed that two media are extended into infinity, and the reference planes are located 10 mm away from discontinuity in both sides. For demonstrating the results on the Smith chart, all parameters are calculated on the metasurface plane.

The first structure is a strip grating, made from metal and illuminated by a wave with parallel polarization (**Figure 3**).

A unit cell of this structure is shown in **Figure 4**. **Table 1** specifies the geometrical characteristics of metasurface element. The frequency variations in reflection and transmission coefficients are plotted in **Figure 4** for this structure.

According to this figure, the major part of incident power is reflected back in medium I.

The frequency variations in S parameters on the Smith chart are demonstrated in **Figure 4**, too. The variations in s_{12} and s_{22} for this structure are the same as the variations in s_{21} and s_{11}, respectively. The dash lines on **Figure 4** are s_{11} and s_{21} circles.

The metallic strips in this structure behave in the same way as parallel inductance in equivalent circuit. **Figure 5** displays the frequency variations in equivalent inductance for the metal grating.

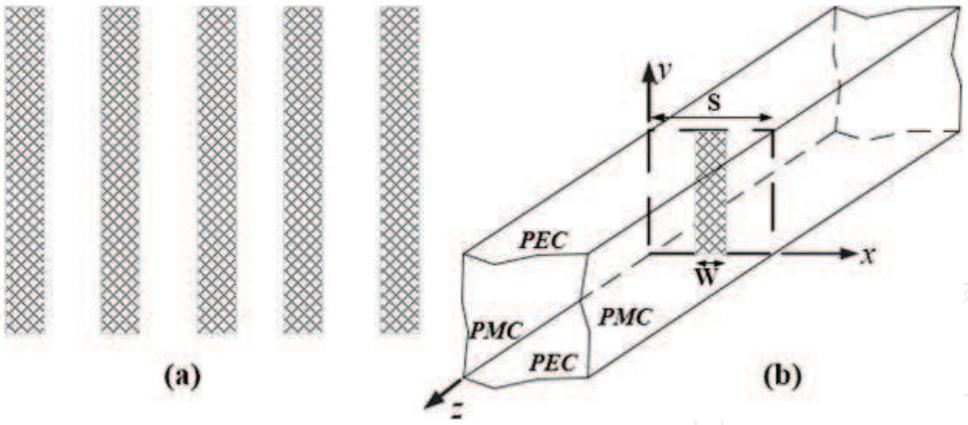

Figure 3. Metal strip grating (a), a unit cell of the structure with suitable boundary conditions in peripheral (parallel polarization) (b) [7].

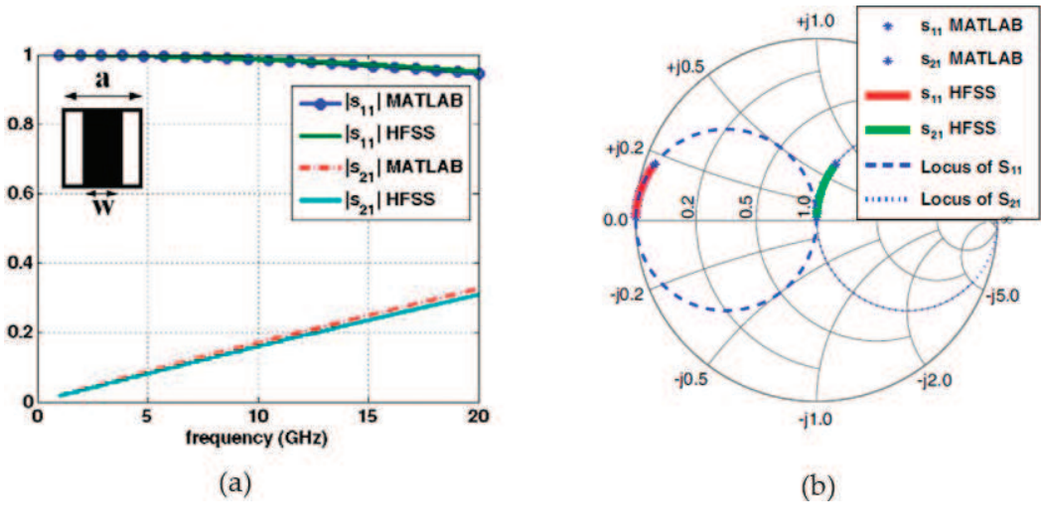

Figure 4. Frequency variations in S parameters for metal strip grating (a) on the Smith chart (b) [7].

a	w	Medium I	Medium II
2.5 mm	0.5 mm	Air	Air

Table 1. Geometrical properties of the metal strip grating (**Figure 5**) [7].

Also, this figure shows the variations in reflection and transmission coefficients versus the width of strip for 10 GHz. According to this figure, the more the parameter w increases, the closer to −1 the parameter $|s_{11}|$ moves. In the limit, when each strip covers all areas of the unit cell, s_{11} goes to −1. In general, with increasing the area of metasurface element, the parameters s_{11} and s_{22} move to −1 along the corresponding circles ($\theta \rightarrow \pi$ in Eq. (16)). Also, the parameters s_{21} and s_{12} move to origin ($\Gamma = 0$) along the corresponding circle (in counterclockwise direction). Note that with decreasing frequency, the parameter θ goes to π for this structure, so that

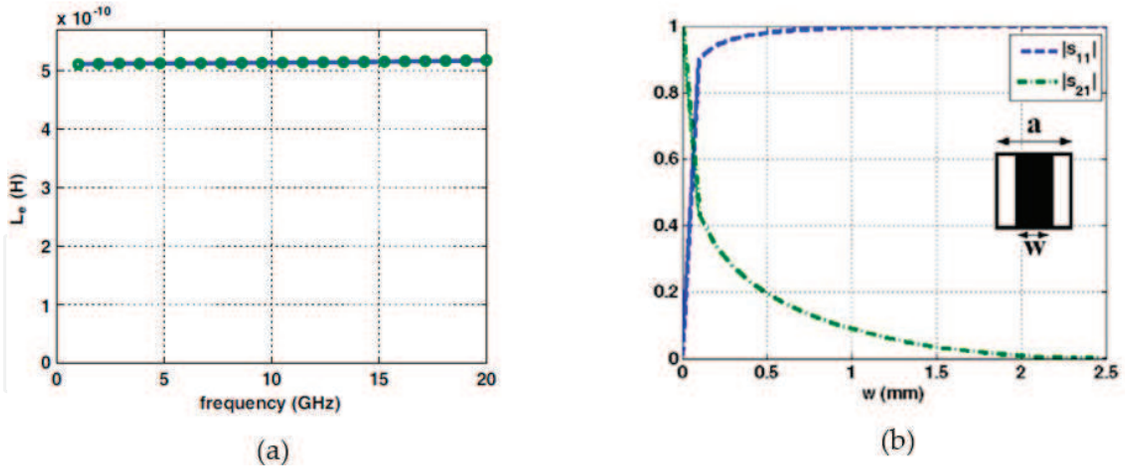

Figure 5. Frequency variations in equivalent inductance (a) and the variation in S parameters versus the width of strip for 10 GHz (b) [7].

when θ equals to π, the value of s_{11} is −1. It is clearly predictable from the model used for simulating metasurface.

The variations in real and imaginary parts of s_{11} versus $|s_{11}|$ are shown in **Figure 6** for this structure. Clearly seen, with increasing $|s_{11}|$ from zero to one, the real part of s_{11} uniformly decreases, while the graph of $Im(s_{11})$ has a maximum where $|s_{11}|$ is equal to $1/\sqrt{2}$ ($\theta = \pi/2$ in Eq. (16)). This point is corresponding to when the excitation of higher-order modes causes the highest stored energy around the structure [7].

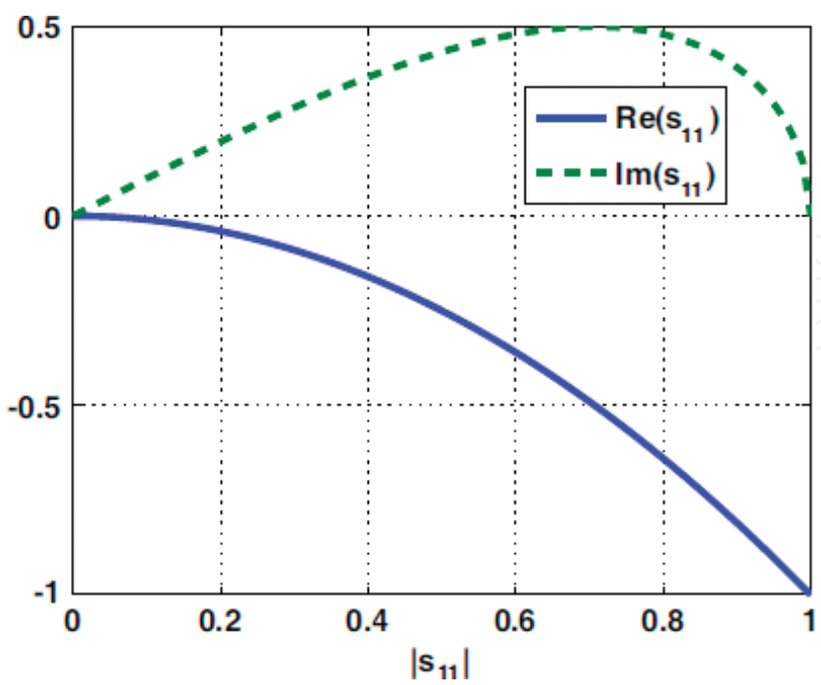

Figure 6. The variations in $Re(s_{11})$ and $Im(s_{11})$ versus $|s_{11}|$ [7].

The second structure is the same as the first example, metal grating printed on Teflon but perpendicular polarization. Physical dimensions of this structure are available in **Table 2**. Simulation results for this structure are demonstrated in **Figure 7**.

According to **Figure 7**, the major part of incident power is transmitted through medium II. **Figure 7** displays the frequency variations in S parameters on the Smith chart for this structure, too. The scattering transfer parameters for this structure are shown in **Figure 8**.

These parameters are located along the straight line [7]. In contrast to the previous structure, the metasurface element in this structure plays the role of parallel capacitance in equivalent circuit. The frequency variations in equivalent capacitance are shown in **Figure 8**. **Figure 9** shows the real and imaginary parts of the reflection coefficient in terms of $|s_{11}|$.

In contrast to what happened about the previous structure, the imaginary part of reflection coefficient is lower than zero, and it has a minimum. This point happens when the stored energy is maximum around metasurface [7]. The variations in the real part of reflection coefficient are similar to the previous structure. Same as the previous structure, the increment in w causes the parameters s_{11} and s_{22} to move to -1 along the corresponding circles. Decreasing and increasing frequency causes s_{11} to move to $((\eta_{00})_{II} - (\eta_{00})_{I})/((\eta_{00})_{II} + (\eta_{00})_{I})$ and -1, respectively.

The next example is a metasurface composed of square patches (**Figure 10**). Let metasurface elements be printed on FR4. Physical dimensions of each element are presented in **Table 3**. **Figure 10** displays simulation results of this structure. The variations in the scattering parameters on the Smith chart are presented in the same figure.

a	w	Medium I	Medium II
2 mm	1.5 mm	Air	Teflon

Table 2. Geometrical properties of the metal strip grating (**Figure 7**) [7].

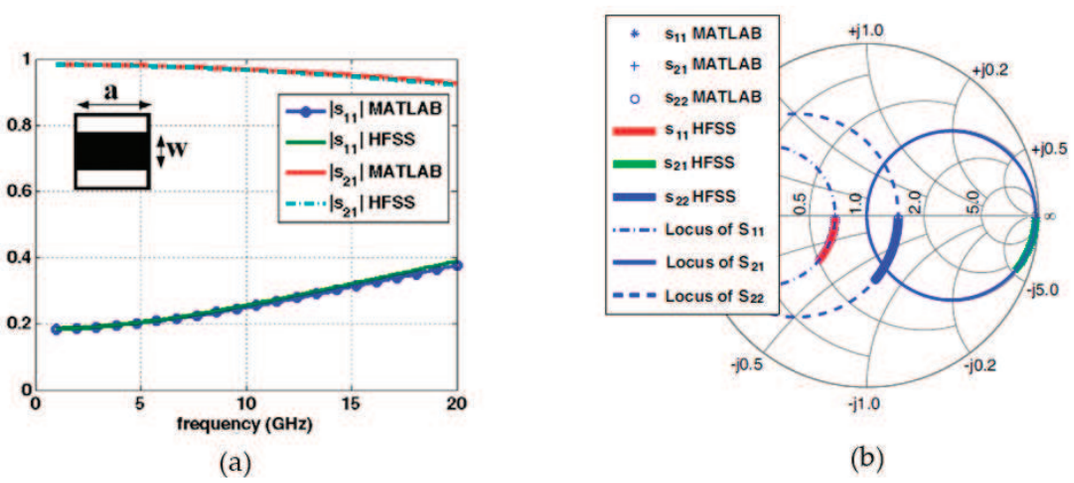

Figure 7. Frequency variations in S parameters for metal strip grating in perpendicular polarization (a) on the Smith chart (b) [7].

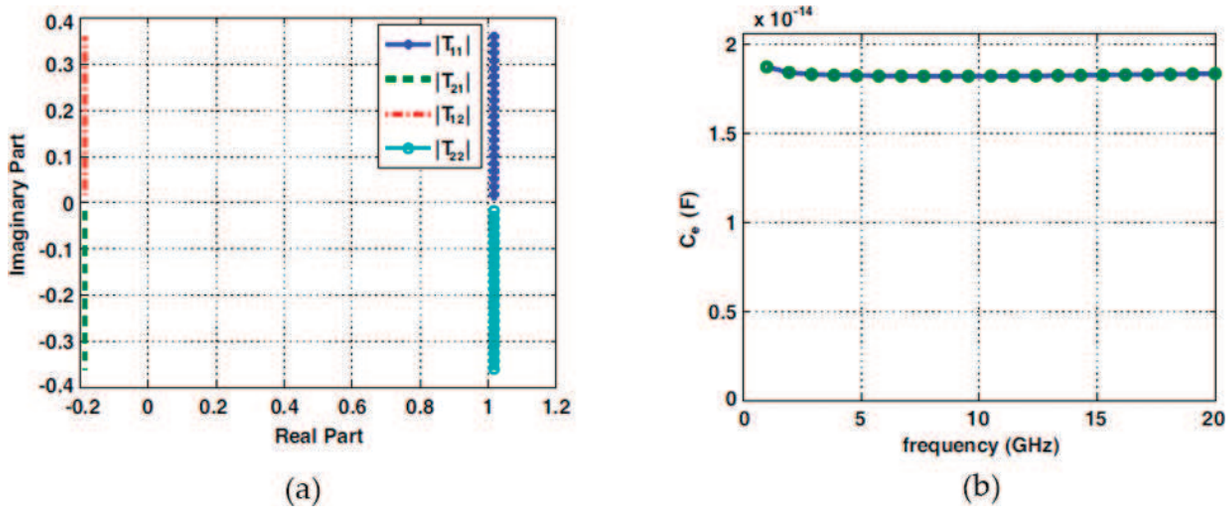

Figure 8. The scattering transfer parameters for metal strip grating (a) and frequency variations in equivalent capacitance (b) [7].

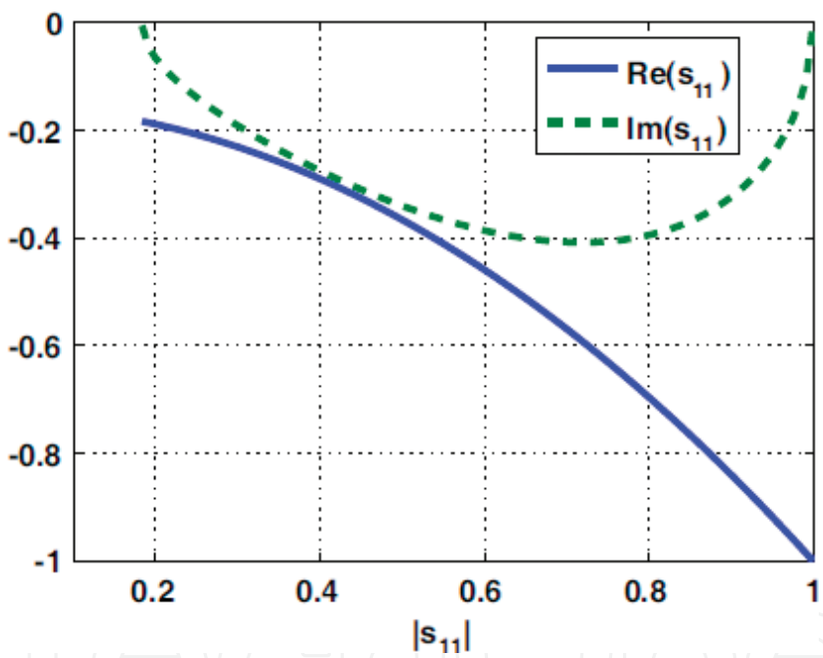

Figure 9. The variations in $Re(s_{11})$ and $Im(s_{11})$ versus $|s_{11}|$ for metal grating in perpendicular polarization [7].

The variations in scattering transfer parameters are demonstrated in **Figure 11** for this structure.

An array of square loops comprises the forth metasurface. This array of loops are located in the boundary between air and FR4. Geometrical properties of each element are available in **Table 4**. Simulation results of this structure are presented in **Figure 12**. The variations in the scattering parameters on the Smith chart are plotted in **Figure 12**.

The variations in scattering transfer parameters are demonstrated in **Figure 13** for this structure.

The last structure is square perforated metal plate. A unit cell of this structure is depicted in **Figure 14**. Suppose that this structure is embedded in air. The geometrical properties of each

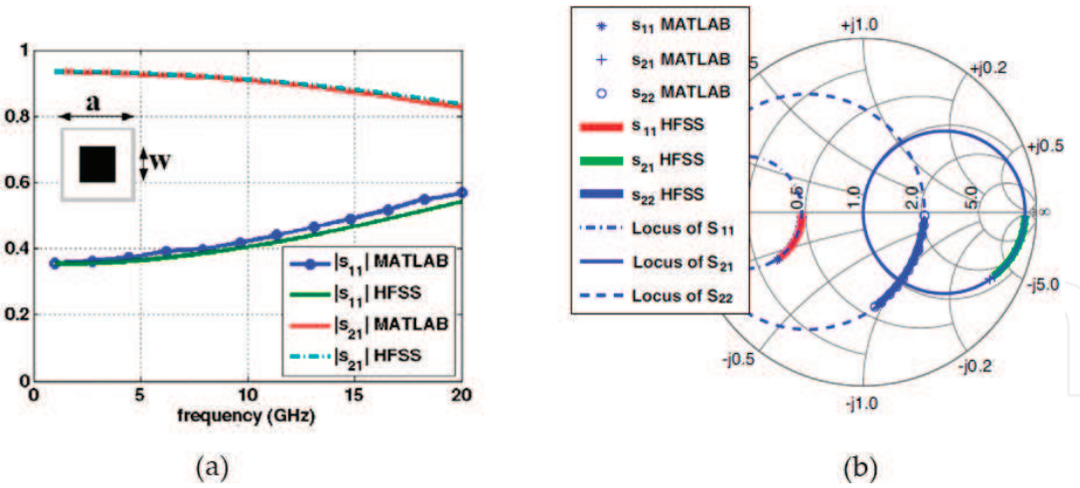

Figure 10. Frequency variations in S parameters for an array of metallic squares (a) on the Smith chart (b) [7].

a	w	Medium I	Medium II
3 mm	2 mm	Air	FR4

Table 3. Geometrical properties of the metasurface comprised from metallic squares [7].

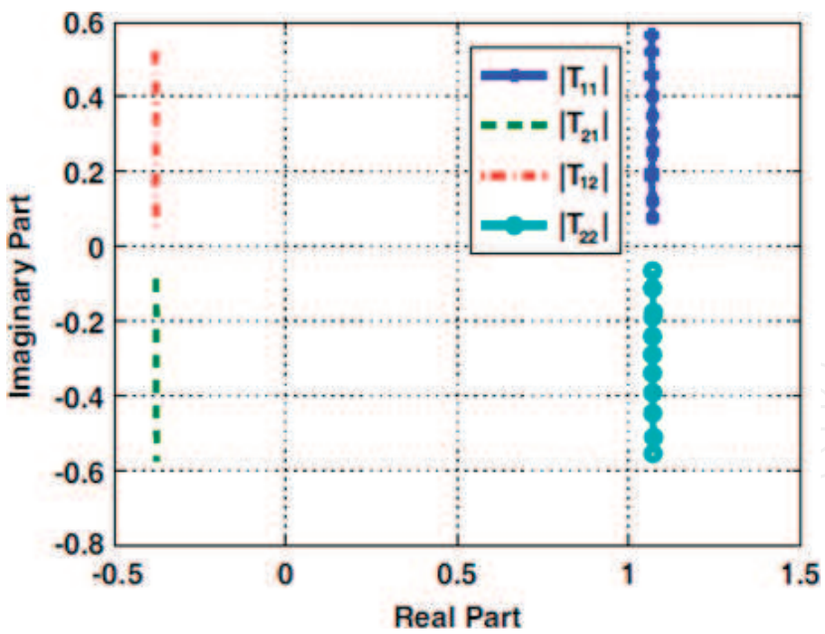

Figure 11. The variations in scattering transfer parameters for an array of metallic squares [7].

element are specified in **Table 5**. The frequency variations in s_{11} and s_{21} for this structure are plotted in **Figure 14**. **Figure 14** shows the variations in S parameters for this structure on the Smith chart.

The variations in scattering transfer parameter corresponding to this structure are demonstrated in **Figure 15**. The variations in S parameters for this metasurface is in the same way of the first structure. The s_{11} for this structure goes to −1 when w increases or frequency decreases. In contrast, increasing the frequency causes the parameter s_{11} to move to 0 along circle.

a	l	w	Medium I	Medium II
1 mm	0.565 mm	0.13 mm	Air	FR4

Table 4. Geometrical properties of the array of metal loops [7].

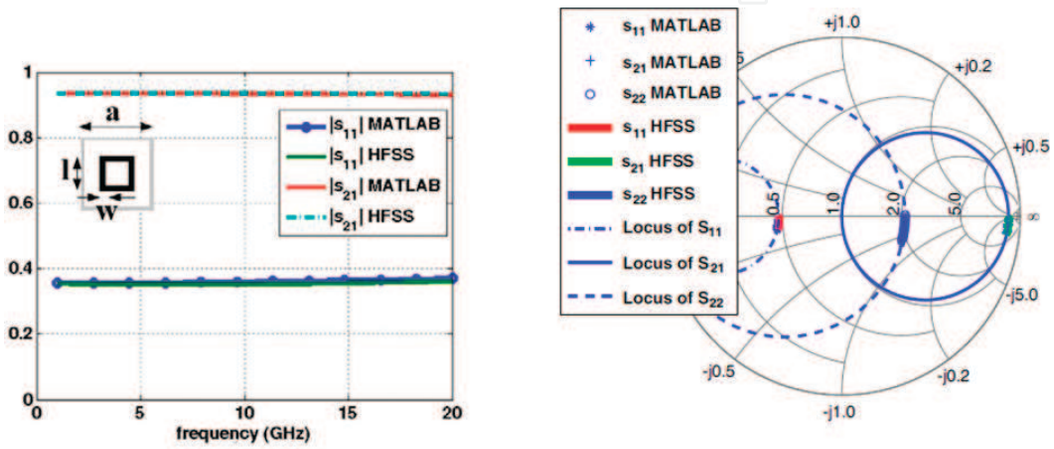

(a) (b)

Figure 12. Frequency variations in S parameters for an array of metal loops (a) on the Smith chart (b) [7].

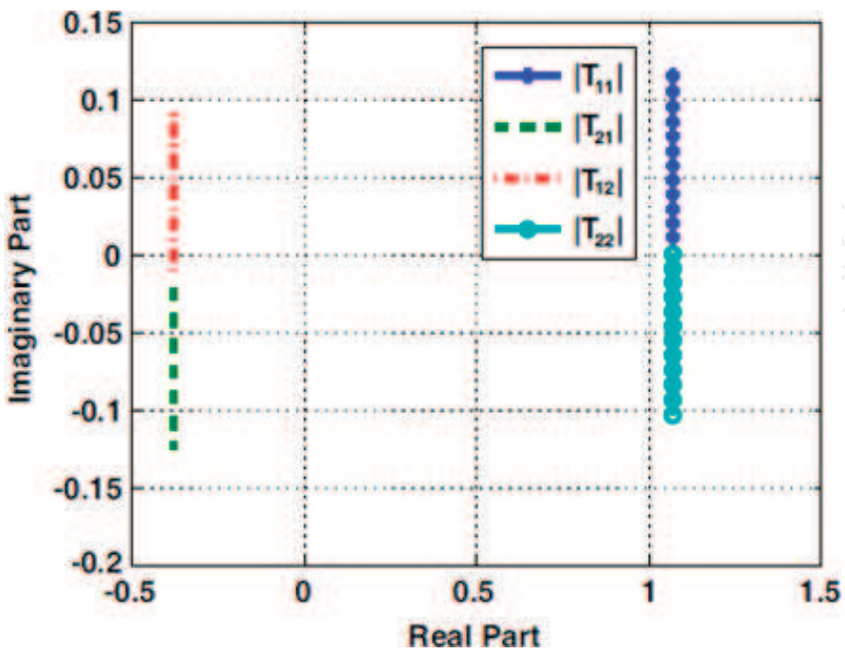

Figure 13. The locus of scattering transfer parameters [7].

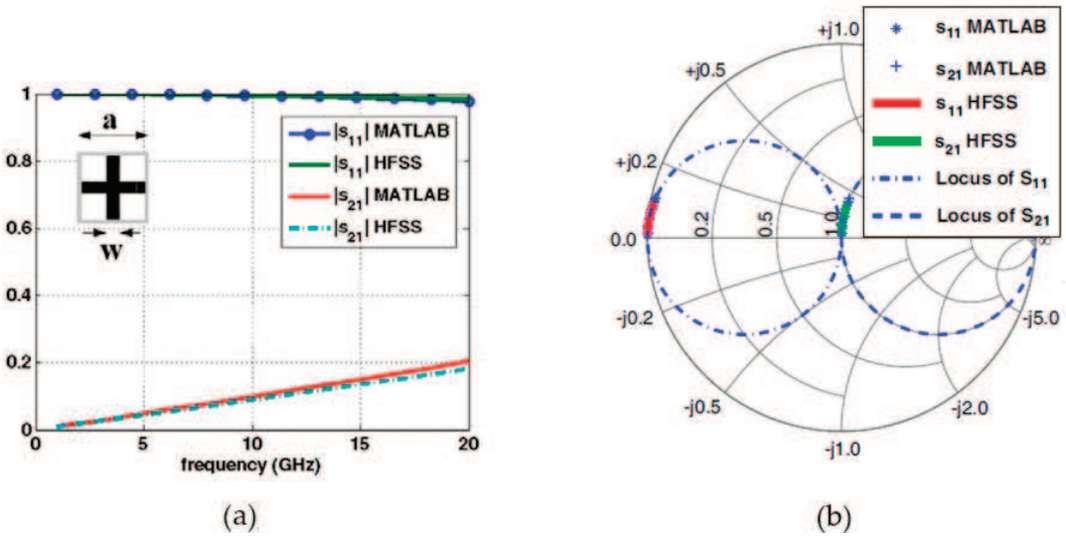

Figure 14. Frequency variations in S parameters for a square perforated metal plate (a) on the Smith chart (b) [7].

a	w	Medium I	Medium II
3 mm	1 mm	Air	Air

Table 5. Geometrical properties of the square perforated metal plate [7].

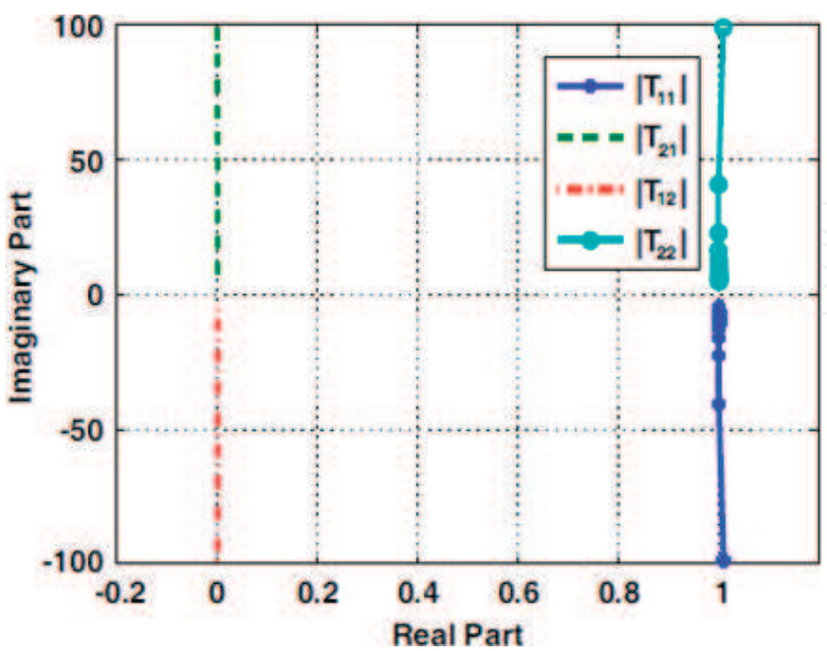

Figure 15. The locus of scattering transfer parameters for the square perforated metal plate [7].

Author details

Mohsen Kalantari

Address all correspondence to: mohsen_kalantari@ymail.com

ICT Research Institute (Iran Research Telecommunication Center), Tehran, Iran

References

[1] Balanis CA. Advanced Engineering Electromagnetics. New York: John Wiley & Sons; 2012

[2] Holloway CL, Kuester EF, Gordon JA, O'Hara J, Booth J, Smith DR. An overview of the theory and applications of metasurfaces: The two-dimensional equivalents of metamaterials. IEEE Antennas and Propagation Magazine. 2012;**54**(2):10-35. DOI: 10.1109/MAP.2012.6230714

[3] Smith DR, Vier DC, Koschny T, Soukoulis CM. Electromagnetic parameter retrieval from inhomogeneous metamaterials. Physical Review E. 2005;**71**(036617):1-11. DOI: 10.1103/PhysRevE.71.036617

[4] Kuester EF, Mohamed MA, Piket-May M, Holloway CL. Averaged transition conditions for electromagnetic fields at a metafilm. IEEE Transactions on Antennas and Propagation. 2003;**51**(10):2641-2651

[5] Holloway CL, Mohamed MA, Kuester EF, Dienstfrey A. Reflection and transmission properties of a metafilm: With an application to a controllable surface composed of resonant particles. IEEE Transactions on Antennas and Propagation. 2005;**47**(4):853-865

[6] Marques R, Mesa F, Jelinek L, Medina F. Analytical theory of extraordinary transmission through metallic diffraction screens perforated by small holes. Optical Express. 2009;**17**: 5571-5579. DOI: 10.1364/OE.17.005571

[7] Meybodi MK, Paran K. Analytical investigation into the S-parameters of metamaterial layers. Progress in Electromagnetics Research B. 2016;**69**:87-101. DOI: 10.2528/PIERB16070806

[8] Huang R, Li ZW, Kong LB, Liu L, Matitsine S. Analysis and design of an ultra-thin metamaterial absorber. Progress in Electromagnetics Research B. 2009;**14**:407-429. DOI: 10.2528/PIERB09040902

[9] Ziolkowski RW. Design, fabrication, and testing of double negative metamaterials. IEEE Transactions on Antennas and Propagation. 2003;**51**(7):1516-1529. DOI: 10.1109/TAP.2003.813622

[10] Hsu CC, Lin KH, Su HL. Implementation of broadband isolator using metamaterial inspired resonators and a T-shaped branch for MIMO antennas. IEEE Transactions on Antennas and Propagation. 2011;**59**(10):3936-3939. DOI: 10.1109/TAP.2011.2163741

[11] Beruete M, Campillo I, Navarro-Cia M, Falcone F, Ayza MS. Molding left- or right-handed metamaterials by stacked cutoff metallic hole arrays. IEEE Transactions on Antennas and Propagation. 2007;**55**(6):1514-1521. DOI: 10.1109/TAP.2007.897324

[12] Bilotti F, Sevgi L. Metamaterials: Definitions, properties, applications, and FDTD based modeling and simulation. International Journal of RF and Microwave Computer Aided Engineering. 2012;**22**(4):422-438. DOI: 10.1002/mmce.20634

[13] Kalantari M, Paran K. Analysing metamaterial layer by simpler approach based on mode matching technique. IET Microwaves, Antennas and Propagation. 2017;**11**(5):607-616. DOI: 10.1049/iet-map.2016.0687

[14] Meybodi MK, Paran K. Straightforward analysis of the effect of any H-plane inductive diaphragm in waveguide. IET Microwaves, Antennas and Propagation. 2017;**11**(5):577-583. DOI: 10.1049/iet-map.2016.0545

[15] Itoh T. Numerical Techniques for Microwave and Millimeter-wave Passive Structures. New York: Wiley Science; 1980

[16] Pozar DM. Microwave Engineering. New York: John Wiley & Sons; 2012

[17] Collin RE. Field Theory of Guided Waves. 2nd ed. New York: Wiley-IEEE Press; 1990

[18] Guglielmi M, Gheri G, Calamia M, Pelosi G. Rigorous multimode network numerical representation of inductive step. IEEE Transactions on Microwave Theory and Techniques. 1994;**42**(2):317-326. DOI: 10.1109/22.275263

[19] Widarta A, Kuwano S, Kokubun K. Simple and accurate solutions of the scattering coefficients of E-plane junctions in rectangular waveguides. IEEE Transactions on Microwave Theory and Techniques. 1995;**43**(12):2716-2718. DOI: 10.1109/22.477852

[20] Wexler A. Solution of waveguide discontinuities by modal analysis. IEEE Transactions on Microwave Theory and Techniques. 1967;**15**(9):508-517. DOI: 10.1109/TMTT.1967.1126521

[21] Ulrich R. Far-infrared properties of metallic mesh and its complementary structure. Infrared Physics. 1967;**7**(1):37-55. DOI: 10.1016/0020-0891(67)90028-0

IntechOpen